Journal of
Applied Crystallography
ISSN 1600-5767

Instrumental setup for high-throughput small- and wide-angle solution scattering at the X33 beamline of EMBL Hamburg

Clement E. Blanchet, Alexey V. Zozulya, Alexey G. Kikhney, Daniel Franke, Peter V. Konarev, Weifeng Shang, Robbert Klaering, Bernd Robrahn, Christoph Hermes, Florent Cipriani, Dmitri I. Svergun and Manfred Roessle

J. Appl. Cryst. (2012). **45**, 489–495

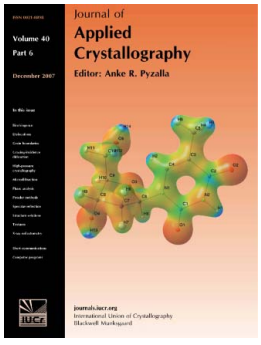

Journal of
Applied Crystallography
ISSN 0021-8898

Received 22 July 2011
Accepted 28 March 2012

Instrumental setup for high-throughput small- and wide-angle solution scattering at the X33 beamline of EMBL Hamburg

Clement E. Blanchet,[a]‡ Alexey V. Zozulya,[a]‡¶ Alexey G. Kikhney,[a] Daniel Franke,[a] Peter V. Konarev,[a] Weifeng Shang,[a] Robbert Klaering,[a] Bernd Robrahn,[a] Christoph Hermes,[a] Florent Cipriani,[b] Dmitri I. Svergun[a]* and Manfred Roessle[a]

[a]EMBL Hamburg, Notkestrasse 85, 22603 Hamburg, Germany, and [b]EMBL Grenoble, 6 rue Jules Horowitz, Grenoble 38042, France. Correspondence e-mail: svergun@embl-hamburg.de

A setup is presented for automated high-throughput measurements of small-angle X-ray scattering (SAXS) from macromolecular solutions on the bending-magnet beamline X33 of EMBL at the storage ring DORIS-III (DESY, Hamburg). A new multi-cell compartment allows for rapid switching between in-vacuum and in-air operation, for digital camera assisted control of cell filling and for colour sample illumination. The beamline is equipped with a Pilatus 1 M-W pixel detector for SAXS and a Pilatus 300 k-W for wide-angle scattering (WAXS), and results from the use of the Pilatus detectors for scattering studies are reported. The setup provides a broad resolution range from 100 to 0.36 nm without the necessity of changing the sample-to-detector distance. A new optimized robotic sample changer is installed, permitting rapid and reliable automated sample loading and cell cleaning with a required sample volume of 40 µl. All the devices are fully integrated into the beamline control software system, ensuring fully automated and user-friendly operation (attended, unattended and remote) with a throughput of up to 15 measurements per hour.

1. Introduction

Small-angle X-ray scattering (SAXS) from biological objects provides information on the low-resolution structure and structural transitions of macromolecules in solution and on the structural organization of bulk materials, *e.g.* fibres, tissues or composites. Novel data analysis methods, particularly suited for the analysis of biological macromolecules in solution, have been developed in the past decade (Svergun & Koch, 2003; Petoukhov & Svergun, 2003; Konarev *et al.*, 2006) and these developments gave rise to a remarkable and continually growing interest within the biological community. A bibliographic search of the PubMed database (http://www.ncbi.nlm.nih.gov/pubmed/) illustrates this enthusiasm well: the number of articles mentioning the terms SAXS or small-angle X-ray scattering in their title or abstract increased drastically over the past decade (63 entries in PubMed in 2000 and 512 in 2010).

To respond to the needs of the growing user community, SAXS instruments have been built at new synchrotron projects such as the SWING beamline at SOLEIL (Paris, France), the SAXS/WAXS (wide-angle X-ray scattering) beamline at the Australian Synchrotron (Melbourne, Australia), I22 at Diamond (Didcot, England), and the SAXS beamlines P12 (BioSAXS) and P03 (MINAXS) at PETRA-III (Hamburg, Germany). Beamline ID14-3 at the ESRF (Grenoble, France) has been transformed from a crystallographic beamline into a SAXS beamline. Beamlines already dedicated to SAXS have been upgraded, in particular by automating the measurements [*e.g.* the SIBYLS beamline at the ALS (Berkeley, USA; Classen *et al.*, 2010) and Beamline 4-2 at the SSRL (Stanford, USA)].

The X33 beamline of the EMBL Hamburg Outstation (Fig. 1), located on a bending magnet of the DORIS storage ring, was among the first dedicated synchrotron SAXS beamlines for biological samples (Koch & Bordas, 1983). Initially it provided high X-ray flux for time-resolved muscle diffraction and kinetic solution scattering experiments. Given the growing demand for SAXS from biological macromolecules, a major upgrade initiated in 2005 (Roessle *et al.*, 2007) enhanced the stability of the beamline, allowing for reliable SAXS experiments using the first dedicated automated sample changer at a solution scattering beamline. This device was built in collaboration with the Fraunhofer Institute IPA (Stuttgart, Germany; Round *et al.*, 2008) and considerably improved the data quality and usability of the beamline setup.

Since the last upgrade, user turnover at the beamline has grown further and X33 currently serves more than 150 user groups per year, mainly from the structural biology commu-

‡ These authors contributed equally to this work.
¶ Current address: HASYLAB at DESY, Notkestrasse 85, 22607 Hamburg, Germany.

nity. A further major upgrade has therefore become necessary to facilitate a more automated and higher-throughput operation and to limit the time needed for beamline maintenance, calibration and change of the experimental setup.

The upgrades performed are described here and include (i) an improved sample environment to switch rapidly between in-vacuum and in-air operations; (ii) a Pilatus multi-detector setup yielding a broader range of scattering vectors by simultaneously recording WAXS patterns; and (iii) integration of a next-generation sample changer for improved speed and reduced sample volume. The technical solutions presented are readily applicable for SAXS/WAXS setups at other high-brilliance synchrotron beamlines. In particular, some of these hardware developments are utilized at the high-brilliance BioSAXS beamline P12 at EMBL, currently being commissioned at the PETRA-III storage ring (DESY, Hamburg).

2. Sample area

A dedicated sample environment is a necessity for biological solution scattering experiments where sample and solvent scattering are measured individually under identical conditions to obtain a solvent-subtracted solute signal. The new vacuum sample environment of X33 was redesigned to meet the following considerations. (i) Operation *in vacuo* is highly desirable to reduce parasitic scattering and air absorption, thus decreasing the background signal (Dubuisson *et al.*, 1997). (ii) The sample cell should be temperature controlled, and should allow for optical monitoring and control of the filling procedure. (iii) It should be easy to connect the setup to the solution sample-handling robots, but it should also provide the possibility of manual sample loading, if needed. (iv) Transformation to an in-air setup for other types of experiment, *e.g.* non-solution scattering studies, should be manageable within a short time frame.

The updated cell compartment consists of a vacuum chamber with four demountable side plates. A vacuum turbo pump and a pressure gauge are connected *via* flanges on the top plate. The chamber houses a position-adjustable cell block and is connected to the beamline tube after the experimental shutter *via* a Ø40 mm bellow. On the back, a flange with a Ø200 mm pendulum valve links the compartment to the front end of the detector flight tube. This valve allows maintenance and manipulations inside the cell compartment without breaking the vacuum of the large detector tube.

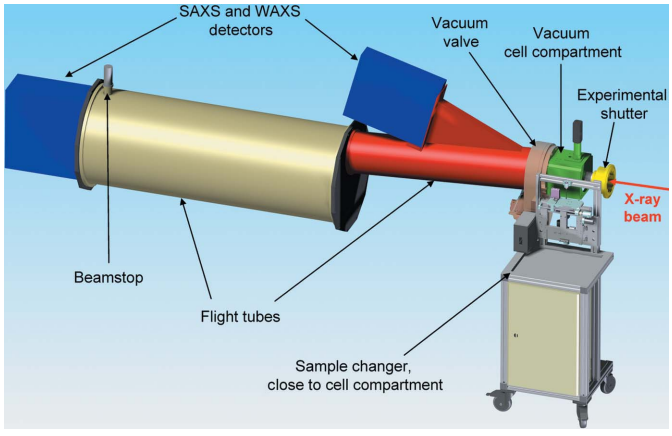

Figure 1
The overall scheme of the major X-ray modules in the experimental hutch of beamline X33. The X-ray beam comes from the right through the experimental shutter (yellow) and enters the vacuum cell compartment (green). The transmitted beam and scattered photons enter the flight tubes (red and cream) and are collected at the two detectors (blue).

2.1. Cell

Two cells were machined in a copper block of 75 × 40 × 8 mm, which was subsequently coated with silver to ensure that the surfaces in contact with the samples are biologically and chemically inert. The profiles were milled using a CNC milling machine, 0.6 mm holes were drilled to access the inflow and outflow of the cells, and a circuit for the thermo-regulating fluid was machined in the block. The temperature of the cell was measured *via* a PT100 thermometer and controlled (between 277 and 333 K) with a water bath (HUBER ministat 125-cc-NR, Huber, Germany). Standard 1/8″ (1″ = 254 mm) vacuum-tight connectors were employed to seal the PTFE tubes through which the samples and thermofluids were guided into the cell block.

The updated design of the measuring cell was inspired by the previous flat cell and has an opening to the X-ray beam of about 7 × 3 mm. The shape of the cell (Fig. 2*a*) minimizes the formation of air bubbles during the filling process: the sample enters the cell from the lower right corner and the air in the chamber leaves through an outlet hole in the upper left corner. The optical path length of the cell is 1 mm, which is optimal for X-ray studies in aqueous solution at the wavelength of 1.5 Å in use at X33 (Feigin & Svergun, 1987). The windows of the cell, either polycarbonate or mica sheet, are held in position by caps equipped with O-rings to ensure cell tightness. The caps also enable easy replacement of the windows when needed. The 125 µm-thick polycarbonate windows (CT301305, Goodfellow GmbH, Germany) allow very good transmission of X-rays (0.92 at 8 keV) but cannot withstand temperatures exceeding 323 K, and also display an elevated (although flat) background scattering at wide angles. Mica has very good mechanical and better thermal properties, and 25 µm-thick windows can be used, at the expense of a lower X-ray transmission (0.75 at 8 keV) than that of the polycarbonate. Because of the low background at wide angles, mica windows are preferred for WAXS experiments. Both types of window were silanated to make the surface more hydrophobic, which improves both filling and cleaning processes. The cell has a volume of 25 µl in air; in vacuum, the pressure exerted on the windows deforms the cell, increasing the volume to about 30 µl.

An additional sealed cell, machined on the block between the two sample cells, contains a silver behenate powder to calibrate the angular axis of the instrument (Huang *et al.*, 1993). This configuration of the cell, with built-in silver behenate, saves a significant amount of time during instrument maintenance, tuning and user measurements.

The cell block is mounted on an *x*–*y* translation stage, allowing the easy positioning of the selected cell in the X-ray

beam and adjustment of its position. Translations are performed by vacuum-compatible compact PP-30 linear stages (PP-30 5805-9-130, miCos GmbH, Eschbach, Germany) driven by piezo motors. They are operated using Beckhoff KL2521 (Beckhoff Automation GmbH, Verl, Germany) modules, which generate steps and direction signals for PMA-100 piezo motor amplifiers (miCos GmbH, Eschbach, Germany). The absolute horizontal and vertical positions are encoded with a linear variable differential transformer (LVDT; 1002XS-D-006, Lukas Schaevitz, USA). The signals from the LDVT and controllers are transferred *via* a Beckhoff bus coupler to a CanBus interface. The design of the translation stage provides accurate backlash-free sample positioning in the range of 30 × 30 mm.

2.2. Monitoring of cell filling

Cell filling is monitored with an on-axis camera, allowing for parallax-free sample viewing through a mirror inclined at 45° with respect to the beam. The sample image is reflected by the mirror and collected by a camera perpendicular to the beam (Fig. 2*b*). The mirror is mounted on a shaft which can be rotated by a 90° pneumatic rotary actuator to free the path for the incident beam during data collection. The sample cell is monitored by an Elphel NC353 high-resolution digital network camera fixed on the top plate outside the cell compartment. The camera is equipped with a front objective by Edmund Optics (OBJ-399911) and is accessible *via* a built-in web server which transfers images on request *via* the standard hypertext transfer protocol. Real-time remote visualization of the cell-filling procedure is possible at 15–30 frames per second.

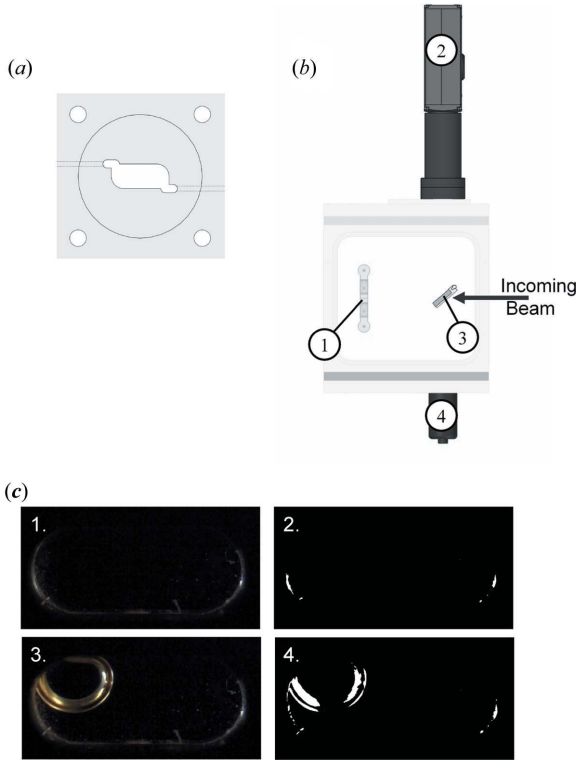

Figure 2
(*a*) In-plane profile of the cell, perpendicular to the beam. The inlet in the lower right corner and outlet at the upper left corner permit stable bubble-free filling of the cell. (*b*) Monitoring systems. The cell block (1) is monitored by a digital camera mounted on the top plate of the cell compartment (2). The image of the cell is recorded with the help of a mirror tilted by 45° (3). A phosphor screen on the back of the mirror can monitor the incoming beam using an analogue camera (4) from the bottom plate. (*c*) Snapshots of properly (1) and improperly (3) filled cells, and the corresponding images [(2) and (4), respectively] obtained after thresholding. The bright area at the air–water interface is emphasized by the threshold and used to detect bubbles.

In addition, the back of the mirror is equipped with a phosphor screen, which can be observed by a second camera through a window in the bottom plate. This allows online inspection of the beam profile and positioning for beam alignment and tuning.

The interior of the cell compartment is illuminated from the back by two sets of standard white LEDs, and a translucent plastic screen is used to achieve diffuse illumination and avoid parasitic reflections. The standard white LEDs can be replaced by monochrome red or blue LEDs, *e.g.* for the study of light-sensitive photoreceptor proteins (Jurk *et al.*, 2010).

The camera allows direct visualization of the cell filling and is used for automated bubble detection, exploiting the high brightness of the air–water interface. An image-recognition algorithm checks for such bright areas and counts pixels whose intensity exceeds a certain threshold (Fig. 2*c*, 1–4). The intensity threshold and the number of intense pixels are predefined parameters which are highly correlated (for instance, a low intensity threshold results in a high number of intense pixels). A calibration algorithm has been designed which counts the high-intensity pixels of an image as a function of the intensity threshold. By comparing the results obtained for images from a correctly filled and a partially filled cell, one can choose an intensity threshold that will give significantly different numbers of pixels for the two cases. The number of intense pixels discriminating between correctly and partially filled cells is chosen.

Several months of use of this bubble-detection system indicate that, once determined, these parameters are very stable, and recalibration is only necessary after mechanical work on the cell or if the colour of the illuminating LED is changed.

A similar algorithm using the bright air–liquid interface and a discriminating threshold is also used at the SIBYLS beamline to detect bubbles; samples with bubbles are then flagged in the user's log file (Classen *et al.*, 2010). The robotic sample changer installed on the X33 beamline (described in §4) also allows for correction of improper cell filling. If a bubble is recognized, the system signals to the control software to hold the exposure, and either informs the user or attempts itself to correct the filling by pulling or pushing the sample. For logging purposes, snapshots of the cell are saved before and after each exposure.

3. Pilatus detector setup

The quality of SAXS data from biological molecules with low scattering contrast crucially depends on the read-out noise of

the detector, and the use of photon-counting detectors with no intrinsic dark current is extremely important for the technique. In the course of the X33 upgrade we have therefore resorted to a new type of hybrid pixel detector, where the X-ray photons are transformed directly into a counting signal. These detector systems, such as the Pilatus from Dectris (Villigen, Switzerland; Broennimann *et al.*, 2006), display no dark current or read-out noise, providing a high dynamic range of 106 photons (20 bits) per pixel and read-out times of less than 3 ms. The modular composition of Pilatus enables flexible assemblies with large active areas ranging from 100 k pixels (one module) to 6 M pixels (60 modules). All these features make Pilatus detectors extremely attractive for synchrotron-based SAXS.

3.1. Pilatus SAXS and WAXS detectors

The detector used for SAXS on the X33 beamline is a Pilatus 1 M-W. It was installed in December 2007 as a 500 k version. This version had five 100 k modules organized vertically in a column to give a total active area of 423.6 × 33.5 mm (2463 × 195 pixels). This strip arrangement of the modules is useful to record isotropic scattering patterns across a wide range. To improve the radial averaging statistics further, the 500 k prototype was upgraded to a ten-module version by adding five more 100 k modules organized in a second parallel column (Pilatus 1 M-W). This enlarged the detector active area to 423.6 × 70 mm (2463 × 407 pixels).

Similar to the SAXS detector, a Pilatus 300 k-W replaced the original gas-filled WAXS detector. The new WAXS detector is composed of three modules arranged in a vertically oriented column, yielding a total active area of 254 × 33.5 mm (1475 × 195 pixels).

3.2. Hardware integration on the beamline

The Pilatus 1 M-W SAXS detector is positioned 2.6 m from the sample, with the beam centre located close to the upper right corner of the active area to measure the scattered radiation along the downward direction. The range of accessible scattering vectors for SAXS, represented by the hatched triangle in Fig. 3, is limited at small angles by the beamstop (10 × 15 mm). For the present setup at X33, the smallest accessible scattering vector q [$q = 4\pi\sin(\theta)/\lambda$, where $\lambda = 1.5$ Å and θ is half the angle between the scattered and direct beams] is 0.06 nm^{-1}, which corresponds to an angle of less than 0.1° and yields about 100 nm resolution (estimated as $2\pi/q$). The SAXS range is limited at high angles by the opening in the flange between the small and large flight tubes. The maximum accessible angle is 8.5°, which corresponds to $q = 6.2$ nm^{-1} (resolution of 1 nm).

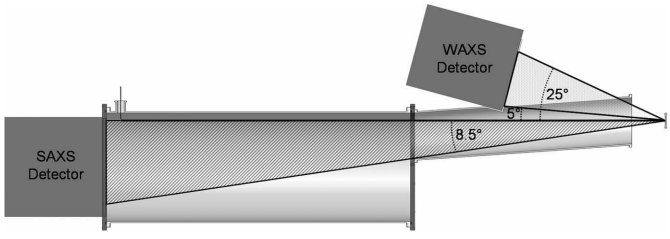

Figure 3
A section of the flight tube. The two detectors, the cell block and the two tubes are shown. The hatched triangle represents the accessible range for SAXS and the dotted triangle that for WAXS.

The WAXS detector is installed on top of the first detector flight tube (Ø200 mm), which was designed to accommodate the Pilatus modules and to increase the accessible WAXS range. The tube is inclined by 4° with respect to the direct beam and the second large flight tube (Ø500 mm). This geometry frees the beam path for photons scattered at wide angles in the upward direction and for the small-angle scattering recorded in the downward direction. The large tube has a rectangular opened flange with a 100 µm-thick Mylar polymer foil as vacuum window, matching the size of the active area of the SAXS Pilatus 1 M-W detector.

The WAXS detector is positioned 0.75 m from the sample and collects photons scattered upwards between 5 and 25°. This results in a range of scattering vectors from 3.7 to 18 nm^{-1}, such that the initial portion of the WAXS patterns overlaps well with the SAXS range. Positioning of the WAXS detector even closer to the sample would not have been feasible as the beam is focused at the SAXS detector position, and thus obtaining even higher angles for WAXS would have led to a noticeable smearing of the WAXS pattern.

3.3. Software integration

The detectors are integrated into the threefold integrated networking environment (TINE), a control system developed in-house at DESY, Hamburg, Germany (Bartkiewicz & Duval, 2007). Separate device servers for the SAXS and WAXS detectors enable simultaneous operation. The data collection is initiated by triggering the detector device server, which initiates subsequent steps such as opening the experimental shutter and starting the collection of monitor values (*e.g.* sample transmission, cell temperature, ring current *etc.*).

The new setup reported here permits simultaneous recording of both SAXS and WAXS patterns with a typical exposure time of 2 min. The data are collected in eight frames of 15 s each. These frames are compared with the first frame taken and checked for radiation damage. Only unaffected files are averaged and passed to the data analysis pipeline.

3.4. Performance of Pilatus detectors

After more than three years of operation we have accumulated ample experience in the use of Pilatus detectors for SAXS data collection. These detectors have revealed excellent performance for solution SAXS applications, being ideally suitable for high-throughput SAXS on synchrotron-based beamlines.

We encountered only a very few problems, one of them being the appearance of 'hot' spots due to malfunctioning amplifiers in individual pixels. The standalone hot pixels are automatically detected and discarded by the processing software, such that only groups of a few pixels had to be masked out by hand. In over three years we have added about 50 bad pixels to the mask file of the Pilatus 1 M-W detector manually, which can be considered very good stability.

Another problem of the Pilatus 1 M-W is related to the variable sensitivity of the different modules, leading to discontinuities in the radially averaged scattering patterns (Fig. 4, filled circles). These effects could not be removed by the available tuning options (energy threshold, standard flat-field correction with the flat field provided by the manufacturer). After trying several different approaches, we found that the easiest way to remove these effects was to perform the sensitivity correction in the binned and radially averaged scattering pattern. The effective sensitivity of the individual bins in the averaged data can be easily assessed from a flat isotropic scattering pattern (*e.g.* that of water) considering the deviations from a smooth curve. These individual sensitivity values are stored in a one-dimensional response function. The computation of the response function is an automated procedure, which is performed (given a high-precision water scattering data set) only once after a beam realignment, together with the detector mask recalculation. The correction results in smooth scattering patterns (Fig. 4, continuous line) and this one-dimensional correction is performed much faster than any two-dimensional correction, being suitable for high-throughput SAXS online analysis and time-resolved data. Of course, this type of response function is only applicable for isotropic scattering data and for the given sample-to-detector distance.

The Pilatus is a practically maintenance-free detector with an extremely high dynamic range and negligible background, which is especially important for SAXS applications. Its advantages are demonstrated in comparing the background stability of the Pilatus 1 M-W with that of a marresearch mar345 image-plate detector. Here, a series of test measurements of water scattering were performed on both detectors during a few hours of a synchrotron run on the X33 beamline. After scaling against the transmitted-beam monitor, these patterns should have coincided with each other, and the fluctuations of the average value at higher scattering angles (in the range $3 < q < 5$ nm^{-1}) provide a good practical measure of the detector background and stability. In the inset of Fig. 4, the average values are presented as functions of the run number, normalized against the first run value for clarity. The uncorrected mar345 data yield a rather high fluctuation level with an r.m.s. deviation of 5.1%, which can be reduced to about 0.6% by a dark-field correction as described by Roessle *et al.* (2007), where the dark-current levels are estimated by masking a portion of the image plate with a lead plate. The Pilatus 1 M-W data, as collected, display a much lower fluctuation level (0.2%), indicating that the detector is fully suitable for precise measurements of high-angle SAXS/WAXS patterns.

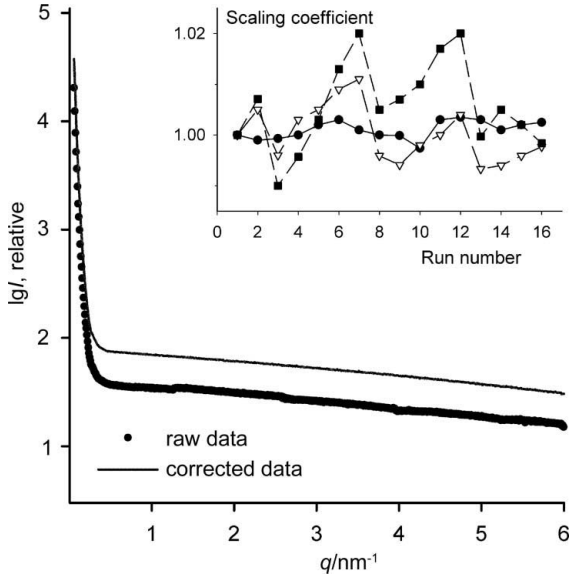

Figure 4
Experimental scattering pattern from water after radial averaging. The circles correspond to raw Pilatus 1 M-W data (with internal flat-field correction only) and the solid line shows the same data after the one-dimensional sensitivity correction. The two curves are offset along the logarithmic axis for clarity. Inset: comparison of the background variation for mar image-plate and Pilatus detectors. Water scattering patterns were recorded on the X33 beamline using the Pilatus detector (filled circles) and the mar image plate [with (open triangles) and without (filled squares) dark-current correction]. After normalization against the transmitted beam, the average values for $3 < q < 5$ nm^{-1} were calculated. They are plotted here, normalized against the first value for clarity.

The data obtained from the SAXS and WAXS detectors are automatically processed and merged by the analysis pipeline at X33 to yield composite scattering patterns. Fig. 5 displays one such composite curve collected in a 2 min exposure time from a protein solution (lysozyme, molecular weight 14 kDa). The data cover a scattering vector range from 0.06 to 17.5 nm^{-1}, corresponding to a resolution between 100 and 0.36 nm. Despite the relatively low protein concentration (5.2 mg ml^{-1}), the data quality is also rather good at wide angles, largely because of the low background of X33 and the absence of dark current in the Pilatus detectors.

4. Sample changer

Several SAXS beamlines are now equipped with automated sample loaders. In some cases, standard liquid-handling devices have been adapted to SAXS stations, such as the SOLEIL SWING beamline with an Agilent HPLC series 1200

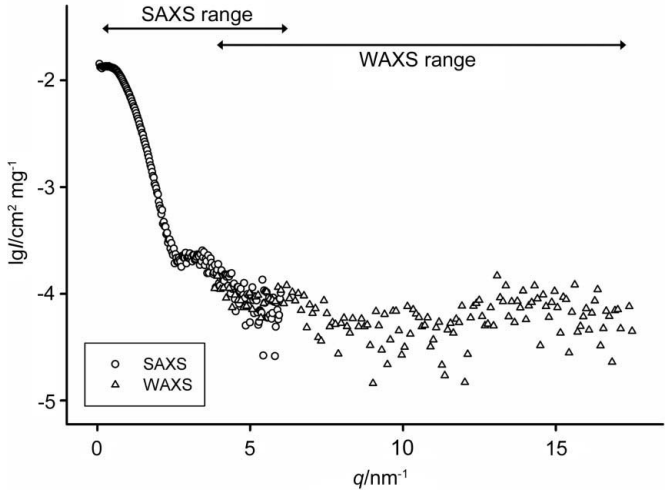

Figure 5
A composite small- (open circles) and wide-angle (open triangles) scattering pattern for lysozyme at 5.2 mg ml^{-1}.

(David & Pérez, 2009) and the SIBYLS beamline at the ALS with a Hamilton MICROLAB 4000 liquid-handling system (Classen *et al.*, 2010). The first dedicated robotic sample changer installed at X33 in 2007 (Round *et al.*, 2008) improved dramatically the entire course of solution SAXS experiments. The automation enabled by this system permits much faster measurements, improves cell cleaning and, very importantly, allows users to monitor the results in real time and to re-plan measurements if required. The reliable operation of the SAXS sample changer has allowed experiments to be performed in unattended or even remote mode, with the possibility of users sending samples in by mail and performing experiments from their offices over the internet (Franke *et al.*, 2012).

The first-generation sample changer was successfully utilized by over 250 external user groups at X33 and proved to be convenient and reliable, but its operation also revealed some problems to be solved. In particular, the robot employed long connecting tubes, which increased filling and cleaning times, leading to undesirable loss of material. The second-generation liquid-handling robot has been designed in a collaboration between EMBL Grenoble, ESRF and EMBL Hamburg for faster operation and reduced sample volume. In the course of this collaboration, a prototype light version of the sample changer has been developed, installed and thoroughly tested in user operation at the X33 beamline.

4.1. Description of the X33 sample changer

In the prototype version (Fig. 6), eight samples and three buffers are stored in a sample tray, the temperature of which is controlled by a water bath (Julabo CF31) and tuneable between 277 and 333 K. The tray is mounted on an x–z stage in order to position the sample under the needle. At the desired position, a sample volume of 40 µl is taken up and delivered into the cell using a motorized syringe. After the measurement, the cell is cleaned with a detergent solution composed of 2% Hellmanex (Hellma Analytics, Muellheim, Germany) and 10% ethanol in water, rinsed with distilled water and finally dried with air. The complete cleaning cycle takes about 45 s, including 25 s of drying time. Optionally, the measured samples can be recovered before cleaning.

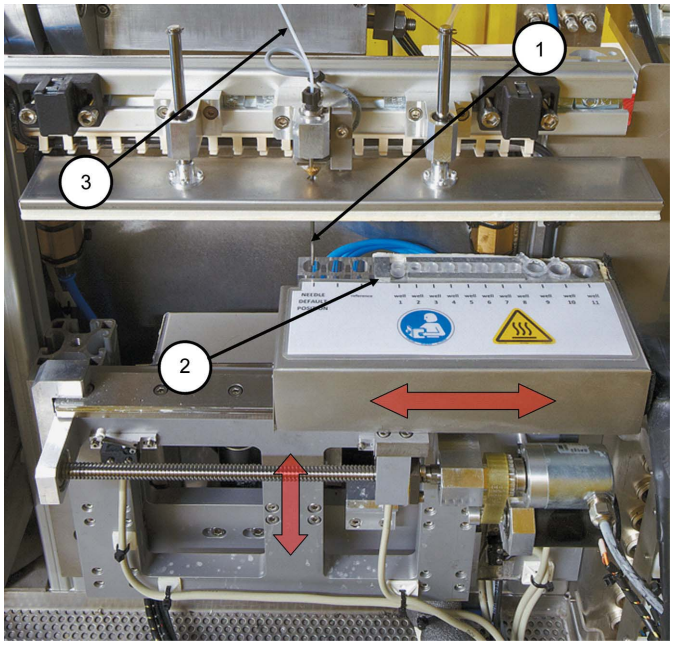

Figure 6
A prototype of the sample changer at the X33 beamline. The sample is delivered to the needle (1) by x–y movements of the thermostated sample tray (2). The liquid is sucked through the tube (3) to the cell using a syringe pump. The needle is kept fixed to minimize the length of tubing between the needle and the cell.

The machine is controlled by Beckhoff EtherCAT electronics and a TwinCAT PLC/NC layer. A Java application implements the device communication and control. The sample changer is connected to the beamline control software *via* a TINE device server and its operation is fully synchronized with the detectors, beamline components and data-processing modules (Franke *et al.*, 2012).

4.2. Performance and comparison with the previous model

The prototype changer installed at the beginning of 2010 was used by over 250 international user groups until the end of 2011. During this period, more than 25 000 full cycles (loading/cleaning/rinsing/drying) were performed. The sample changer worked very reliably on a wide variety of samples, including rather viscous samples of fibrillating proteins and buffers with low viscosity such as methanol.

The time needed for a sample-changer cycle (filling and washing) decreased from about 4–5 min for the original sample changer to less than 2 min for the new prototype, allowing up to 15 samples per hour to be measured at X33 (with a collection time of 2 min). The sample volume required also decreased from 80 to 40 µl, which is an important step towards high-throughput SAXS screening.

These new features of the sample changer significantly improved the performance and usability compared with the previous model. The technical solutions for ensuring these advanced options are, in particular, (i) the needle is kept fixed and the samples are delivered to the needle, which requires only short tubing between the needle and the cell; and (ii) a motorized syringe is used for sample transfer, which allows high accuracy for sample positioning, fine control of the flow for bubble-free filling, recovery of the sample and, potentially, measurements under continuous flow.

The cell cleaning proved to be very efficient and extended the lifetime of the cell windows. Indeed, during manual operation the windows had to be changed two or three times per week. With the first robot in operation, the lifetime increased to about a week, and with the new machine the windows can be typically kept for over two weeks without significant deterioration in data quality. Nevertheless, the availability of the two measuring cells described in §2 was very useful, with users having the possibility of switching rapidly to another cell in the case of *e.g.* window fracture during the night shift.

The evaluation setup of the new sample changer can only store eight samples and three buffers. Therefore, the previous sample changer is still employed at X33 for remote experi-

ments because of its storage capacity (192 samples and 48 buffers). The final version of the second-generation robot, already in operation at the ESRF and at the BioSAXS beamline at PETRA-III, uses the same loading and cleaning procedures as the above-described prototype but has an increased capacity, with a total of 288 samples and buffers.

5. Conclusion

Given the versatility and wide range of applications of SAXS, most synchrotron SAXS beamlines are multipurpose, allowing users to measure different types of sample under variable conditions. This versatility is sometimes an obstacle for high-throughput studies, because new users have to spend part of their allocated time setting up the environment and tuning and configuring the beamline. The X33 beamline is largely dedicated to and optimized for solution-scattering experiments on biological samples. The experimental setup covers a wide SAXS/WAXS range without changing the sample-to-detector distance or other retuning. The vacuum cell setup provides the optimum conditions for solution SAXS. For users with other types of bulk samples (powders, solids, thick gels, fibres *etc.*), which require an in-air environment, the cell compartment has been redesigned in such a way that the transition can be rapidly performed. Complete disassembly of the vacuum setup requires just the removal of the vacuum components and their replacement by flanges. Conversion to the in-air setup and back is done within 1–2 h and does not require any beamline realignment. Nevertheless, given the high user load, in-air experiments are scheduled in blocks (a few per year), so that most of the experiments start without any delay at all.

Over three years' experience in the use of Pilatus detectors leads us to the (not entirely unexpected) conclusion that they are presently the best X-ray detectors for solution-scattering experiments. Their absence of dark current, high dynamic range and maintenance-free operation are among the major factors. The readout time (about 3 ms) is sufficiently fast for static and most kinetic SAXS studies, although specific experiments such as time-resolved muscle diffraction may require yet faster detectors (Lewis *et al.*, 2000).

The automated sample changers described here have revolutionized data-collection procedures in biological solution SAXS, allowing for high-throughput studies. The prototype of the second-generation sample changer implemented at X33 provides even more reliable and faster operation and reduced sample volumes compared with the initial machine (Round *et al.*, 2008). The prototype we tested has a limited storage capacity, but such a small machine would be fully appropriate for the automation of solution experiments on laboratory X-ray cameras, where the measurement of eight samples may take the entire working day.

All hardware components of the beamline are fully integrated and controlled by a beamline meta server (Franke *et al.*, 2012) using the TINE software to allow for completely automated data collection in attended, unattended and remote modes. The obtained data are processed and analysed by an automated analysis pipeline, yielding the structural parameters and even three-dimensional low-resolution models in real time (Franke & Svergun, 2009). The developments described in the present paper have made it possible to perform high-throughput solution-scattering measurements at X33. This beamline has simultaneously served as a test bed for the construction of the high-brilliance undulator BioSAXS beamline of EMBL at the PETRA-III storage ring, presently in the commissioning phase. Many approaches tested at X33 have been implemented at the BioSAXS beamline, and the experience reported here may be useful for other synchrotron beamlines with a strong component of solution-scattering SAXS.

The authors thank U. Ristau, D. Jahn and T. Gehrmann for valuable technical advice and support. We also thank Lukas Foedinger, Alexandre Gobbo, Julien Huet, Franck Felisaz, Raphael Moya, Cyril Villard and Adam Round (EMBL Grenoble), as well as Petra Pernod (ESRF), who were involved in the development of the sample changer. We acknowledge funding from the EU FP6 Infrastructures Program, Design Study grant SAXIER, RIDS contract No. 011934, the EU FP7 e-Infrastructures Program, grant WeNMR, contract No. 261572, and the BMBF research grant SYNC-LIFE, contract No. 05K10YEA. We thank P. Broennimann (Dectris) for providing the custom-made Pilatus 500 k-W version of the detector and for help in its operation and upgrade.

References

Bartkiewicz, P. & Duval, P. (2007). *Meas. Sci. Technol.* **18**, 2379–2386.
Broennimann, Ch., Eikenberry, E. F., Henrich, B., Horisberger, R., Huelsen, G., Pohl, E., Schmitt, B., Schulze-Briese, C., Suzuki, M., Tomizaki, T., Toyokawa, H. & Wagner, A. (2006). *J. Synchrotron Rad.* **13**, 120–130.
Classen, S., Rodic, I., Holton, J., Hura, G. L., Hammel, M. & Tainer, J. A. (2010). *J. Synchrotron Rad.* **17**, 774–781.
David, G. & Pérez, J. (2009). *J. Appl. Cryst.* **42**, 892–900.
Dubuisson, J.-M., Decamps, T. & Vachette, P. (1997). *J. Appl. Cryst.* **30**, 49–54.
Feigin, L. Q. & Svergun, D. I. (1987). *Structure Analysis by Small-Angle X-ray and Neutron Scattering*, pp. 22–23. New York: Plenum Press.
Franke, D., Kikhney, A. & Svergun, D. I. (2012). In preparation.
Franke, D. & Svergun, D. I. (2009). *J. Appl. Cryst.* **42**, 342–346.
Huang, T. C., Toraya, H., Blanton, T. N. & Wu, Y. (1993). *J. Appl. Cryst.* **26**, 180–184.
Jurk, M., Dorn, M., Kikhney, A., Svergun, D., Gärtner, W. & Schmieder, P. (2010). *J. Mol. Biol.* **403**, 78–87.
Koch, M. H. J. & Bordas, J. (1983). *Nucl. Instrum. Methods Phys. Res.* **208**, 461–469.
Konarev, P. V., Petoukhov, M. V., Volkov, V. V. & Svergun, D. I. (2006). *J. Appl. Cryst.* **39**, 277–286.
Lewis, R. A., Berry, A., Hall, C. J., Helsby, W. I. & Parker, B. T. (2000). *Nucl. Instrum. Methods Phys. Res. Sect. A*, **454**, 165–172.
Petoukhov, M. V. & Svergun, D. I. (2003). *J. Appl. Cryst.* **36**, 540–544.
Roessle, M. W., Klaering, R., Ristau, U., Robrahn, B., Jahn, D., Gehrmann, T., Konarev, P., Round, A., Fiedler, S., Hermes, C. & Svergun, D. (2007). *J. Appl. Cryst.* **40**, s190–s194.
Round, A. R., Franke, D., Moritz, S., Huchler, R., Fritsche, M., Malthan, D., Klaering, R., Svergun, D. I. & Roessle, M. (2008). *J. Appl. Cryst.* **41**, 913–917.
Svergun, D. I. & Koch, M. H. J. (2003). *Rep. Prog. Phys.* **66**, 1735–1782.